Advanced Method for the Reliable Estimation of Spin-Orbit-Torque Efficiency in Low-Coercivity Ferromagnetic Multilayers

Maksim E. Stebliy,[1] Alexander G. Kolesnikov,[1] Alexey V. Ognev,[1] Aleksandr V. Davydenko,[1]
Ekaterina V. Stebliy,[1] Xiao Wang,[2] Xiufeng Han,[2] and Alexander S. Samardak[1,3,*]

[1]*School of Natural Sciences, Far Eastern Federal University, Vladivostok 690950, Russia*
[2]*Beijing National Laboratory for Condensed Matter Physics, Institute of Physics, Chinese Academy of Sciences,
Beijing 100190, China*
[3]*National Research South Ural State University, Chelyabinsk 454080, Russia*

The reliable estimation of the spin-orbital-torque (SOT) efficiency in ferromagnetic multilayers with small coercive force is a nontrivial task, but extremely demanded for implementation of current-induced magnetization reversal memory cells. Here, we report on results of an experimental study of current-induced magnetization reversal of the Ru/Co/Ru and Ru/Co/Ru/W structures. In the considered structures, because of the small value of the coercive force comparable in magnitude to the Oersted field and the SOT effect field, the magnetization reversal is carried out by moving a domain wall parallel to the direction of current injection. For such a case, an alternative method for estimating the effective field of SOT based on the analysis of the domain-wall position considering the distribution of the Oersted field is proposed. This method allows us to determine the effective longitudinal field $\mu_0 H_L/j = 1.6 \times 10^{-11}$ mT/Am^{-2} and the efficiency of SOT $\xi_L = 0.03$ in the quasisymmetric Ru/Co/Ru structure. An addition of a capping layer of W enhances ξ_L by 5 times.

I. INTRODUCTION

The development of a reliable method for the local control of the magnetization is one of the key directions in the development of spintronics. A promising method is the current-induced switching of the magnetization in systems with a strong spin-orbit interaction due to the spin-orbit torque (SOT) [1]. This method is currently used for realization of memory cells, logic, and neuromorphic devices [2–5]. This effect may be due to the spin Hall effect (SHE) and the Rashba effect (RE) and is usually realized in structures with perpendicular magnetic anisotropy (PMA) and broken inversion symmetry [6]. The simplest way to create such an asymmetry in order to realize deterministic magnetization switching is to apply an external in-plane magnetic field. In recent years, an active study of this mechanism has been aimed at searching for structures and optimizing process parameters, which make it possible to achieve maximum efficiency of current-induced magnetization reversal, as well as a theoretical explanation of the SOT effect mechanism.

To implement the SOT effect, three-layer structures consisting of a heavy-metal (HM) buffer layer with a strong spin-orbit interaction, a ferromagnetic layer (FM),

and a capping layer preserving oxidation and PMA are usually used. As a buffer, $5d$ metals are mainly used (Pt, Ir, W, Ta, Hf) due to a combination of a large spin Hall effect and a small spin diffusion length (λ_{sd}) [7–9]. For this reason, structures containing $4d$ metals, for example, Ru or Pd, are much less studied [10,11]. One of the ways to enhance the efficiency of current-induced magnetization reversal is the combination of various heavy metals, which can lead to an increase in the spin current density injected into the FM layer. Previously, structures with FM sandwiched between a pair of HM were studied: Pt-Ta [12] or Pt-W [13]. As criteria for evaluating efficiency, the following parameters are usually chosen: the magnitude of longitudinal (antidampinglike) or transverse (fieldlike) fields ($\mu_0 H_{L/T}$) generated by the SOT effect [14,15]; the magnitude of the critical magnetization reversal current (I_c) [16]; and the effectiveness of the SOT effect (ξ_j) [17]. A general method for determining the magnitude of the effective magnetic field induced by the SOT effect is the harmonic approach based on calculation [17] or fitting [18]. There are other estimation methods, for example, the current-induced hysteresis-loop-shift method [19] or the approach based on the measurement of magnetization curves [20].

In this paper, an alternative method of a direct estimation of the SOT fields in low-coercive (H_c values are

_____
[*]samardak.as@dvfu.ru

in an approximate range from 1 to 10 mT) structures by the position of a domain wall is proposed. In addition to SHE and RE, as a result of the current passing through a Hall bar, the Oersted field is generated, which is responsible for initiating the reversal process [21,22]. Accounting for this field is especially important when considering systems with low coercive force. In this work, we compare the effective longitudinal field ($\mu_0 H_L$) and the SOT efficiency (ξ_L), which is an effective angle of SHE, determined by three different methods: (i) second harmonics, (ii) current-induced magnetization curve, and (iii) domain-wall position.

II. EXPERIMENTAL PROCEDURES

In a previous study, we showed that the magnetic parameters of Co, such as the coercive force and the PMA energy, in quasisymmetrical Ru/Co/Ru films can vary over a wide range of values by changing the thickness of the FM and HM layers [23]. Such a possibility could make this system interesting for studying the dependence of the current-induced magnetization reversal effect on the magnitude of the magnetic parameters. In previous studies, it was shown that even in symmetric structures, for various reasons, as a result of the SOT effect, a nonzero effective field can be generated, which is sufficient for the magnetization switching [24,25]. However, experimental studies have shown that the effectiveness of SOT in such a system is small, as is shown below. To increase the efficiency in the considered structure, a capping layer of W was added. On one hand, W has a large SHE angle (Θ_{SH}) compared to Ru: -0.18 and $+0.006$ for W and Ru, respectively [10,26]. On the other hand, W has the same as the Ru sign of Θ_{SH} when these materials are placed from different sides of a ferromagnet. It leads to the summation of the spin currents from the bottom and top interfaces [Fig. 1(a)]. Our experimental studies have shown that the presence of an ultrathin Ru interlayer between Co and W is a necessary condition for the preservation of PMA. The minimal possible thickness of the Ru interlayer, at which PMA is still induced, is 1.2 nm. We suggest that a Ru interlayer of this thickness should not be a source of spin polarized current, since its thickness is less than the spin diffusion length in Ru (4 nm) [27,28].

At nanometer thicknesses, the W layer can be in an amorphouslike, α-(bcc), or β-(A15 cubic) phase [29], for which the value of Θ_{SH} is very different: 0.23, 0.07, and 0.4, respectively [26,30,31]. Depending on the structure and parameters of the experiment, the β-phase can form in the W thickness range up to 26 nm [32], but it has been defined experimentally that the largest Θ_{SH} value usually lies in the interval from 2.5 to 9 nm [13,31]. The quantitative criterion for estimating the type of phase can be the value of resistivity: for the α-phase it is from 20 to 40 $\mu\Omega$ cm and for the β-phase it is from 120 to 260 $\mu\Omega$
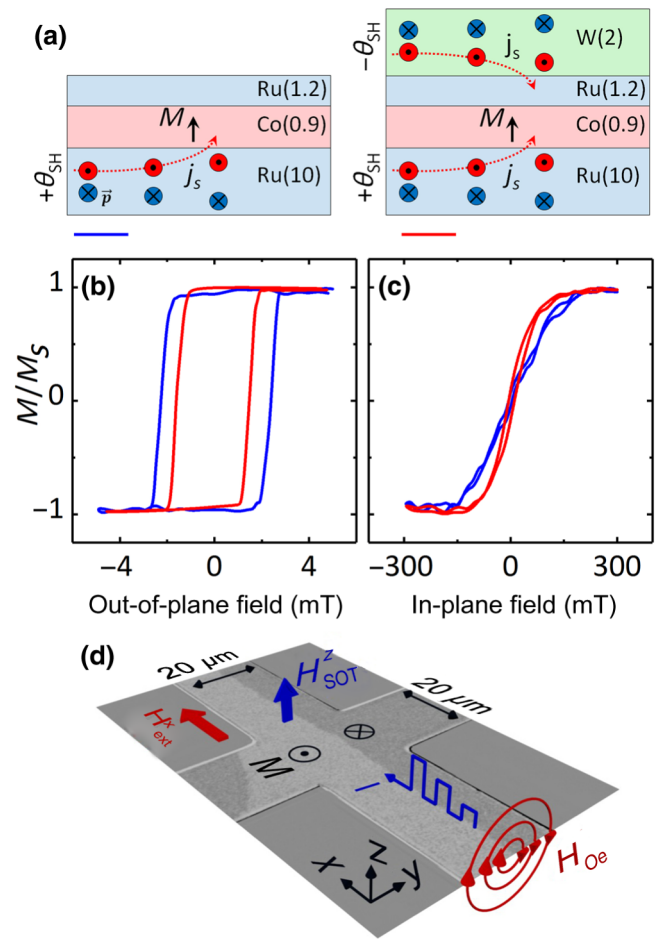

FIG. 1. (a) Schemes of experimentally studied multilayer structures (thicknesses in nm). The red arrows indicate the direction of the spin-current injection from Ru and W layers. Magnetic hysteresis loops measured with VSM during remagnetization in an external magnetic field applied perpendicular (b) and parallel (c) the sample plane. (d) Kerr image of the Hall bar under study with a schematic indication of the relative orientation of the magnetization (**M**), external field ($\mu_0 H_{ext}^x$), passing current (I), Oersted field ($\mu_0 H_{Oe}$) induced by this current, and effective field of SOT ($\mu_0 H_{SOT}^z$).

cm [13,26,32]. Intermediate resistivity values correspond to the metastable β-phase [33] or the mixed $\alpha + \beta$ phase, for which Θ_{SH} can take an intermediate value of approximately 0.18 [26]. We determine the phase of W by the resistivity measurement.

We measure the specific resistance of the W capping layer for the series of Ru(10)/Co(0.9)/Ru(1.2)/W(t_W) samples, where t_W changes from 0 to 8 nm [Fig. 2]. Comparing the obtained values of the specific resistance with the literature data, we can conclude that the W layer is in the mixed $\alpha + \beta$ phase. It was determined experimentally that a sharp increase in the efficiency of current-induced magnetization reversal, as compared with the Ru/Co/Ru structure, is observed up to $t_W = 2$ nm. A further increase
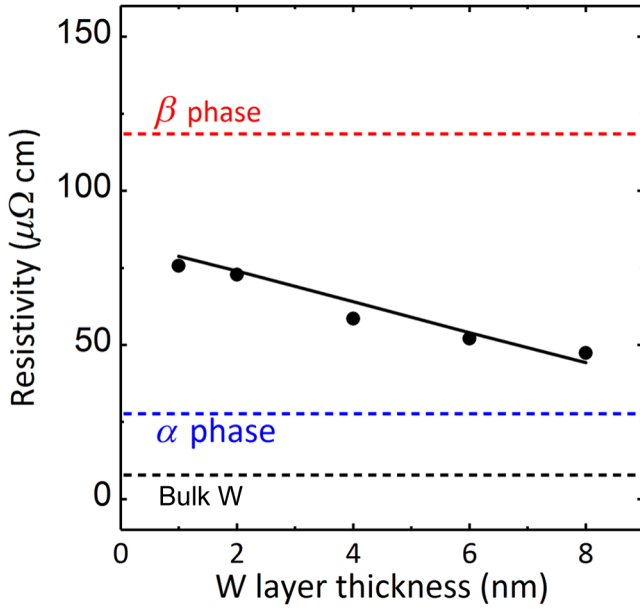
FIG. 2. Experimental values of the specific resistance of the W capping layer in Ru(10)/Co(0.9)/Ru(1.2)/W(t_W) structures. The dotted line in the graph shows the average values of the specific resistance corresponding to α and β phases, as well as to the bulk W taken from the literature data.

TABLE I. Magnetic parameters of Ru(10)/Co(0.9)/Ru(1.2) and Ru(10)/Co(0.9)/Ru(2) films.

Parameters	Ru/Co/Ru	Ru/Co/Ru/W
M_s (A/m)	1.1×10^6	1.1×10^6
$\mu_0 H_k^{\text{eff}}$ (mT)	140	60
K_{eff} (J/m^3)	7.7×10^4	3.3×10^4
$\mu_0 H_c$ (mT)	2.2	1.6

the addition of the W layer, the magnitude of the saturation magnetization M_s does not change, whereas the value of the coercive force $\mu_0 H_c$ and the energy of effective anisotropy K_{eff} (or the field $\mu_0 H_k^{\text{eff}}$) change two or more times. In Ru/Co/Ru films, the magnetoelastic anisotropy makes the main contribution to PMA [23]. It can be assumed that W atoms penetrate into the Ru layer due to their high diffusion capacity and form impurity dislocations, reducing the stresses in the Ru/Co interface, which results in the effective PMA and coercive force decrease [35,36].

III. RESULTS AND DISCUSSION

A. Current-induced magnetization reversal

To study current-induced magnetization reversal, current pulses are passed through the Hall bars with a maximum amplitude of ± 60 mA and a duration of 7 ms in the presence of a planar field $\mu_0 H_{\text{ext}}^x = -8, \ 0, \ +8$ mT. The value of the field 8 mT is chosen because, for the structure containing W in this field, a complete switching of the magnetization begins to be observed. Passing the current leads to the generation of two fields: the Oersted field $\mu_0 H_{\text{Oe}}$, which has a nonuniform profile and a different orientation at opposite edges, and the effective field induced by the SOT effect $\mu_0 H_{\text{SOT}}^z$, which is uniform across the entire microstrip [Fig. 1(d)]. The change in magnetization is recorded using Kerr microscopy or by measuring the anomalous Hall effect (AHE), while passing the current of 1 mA. The potential difference resulting from AHE is proportional to the perpendicular component of the magnetization.

For the convenience of visualization and further analysis, the effect of the current on a sample preliminarily magnetized to the saturation state is considered. We conduct the following sequence of measurements:

1. Current-induced magnetization reversal in the absence of an external field $\mu_0 H_{\text{ext}}^x$

Initially, the samples are magnetized by an external magnetic field $\mu_0 H_{\text{ext}}^z$ to a saturation state with $\pm M_s$. After that, in the absence of an external magnetic field, current pulses with amplitude from 0 to ± 60 mA with a step of 2 mA are applied. After each pulse, the AHE value is measured. The current density is not greater than

in the W thickness leads to a slight linear enhancement in the magnitude of the effective fields induced by the current. Thus, the sharp increase in the SOT efficiency is completed when t_W is comparable to the spin diffusion length, which for W lies in the range from 1.1 to 3.5 nm [31,34].

Experimental samples based on Ru/Co/Ru films are prepared by magnetron sputtering on an oxidized SiO2 silicon substrate. The base pressure in the vacuum system is 1.3×10^{-6} Pa; DC sputtering of all materials is carried out in the Ar atmosphere of pressure of 0.5 Pa at room temperature. The deposition rates of materials are 0.07 nm/s for Co, 0.02 nm/s for Ru, and 0.05 nm/s for W. For the study of current-induced magnetization reversal, Hall bars with a size of $20 \times 200 \ \mu m^2$ are prepared using the photolithography and lift-off procedure [Fig. 1(d)]. The magnetic parameters of the structures are measured using a vibration sample magnetometer (VSM 7410, LakeShore). Current-induced magnetization reversal is investigated at a probe station equipped with electromagnets inducing in-plane ($\mu_0 H_{\text{ext}}^x$) and out-of-plane ($\mu_0 H_{\text{ext}}^z$) fields, together with a Keithley 2182a voltmeter and a Keithley 2420 current source. The current-induced magnetization reversal process is visualized using a Kerr microscope.

In this paper, we study the effect of current on the magnetization in two structures: Ru(10)/Co(0.9)/Ru(1.2) and Ru(10)/Co(0.9)/Ru(1.2)/W(2), with thicknesses in nanometers. The magnetic parameters of the prepared samples, measured for the corresponding films, are given in Table I. Comparing the results, it can be noted that with
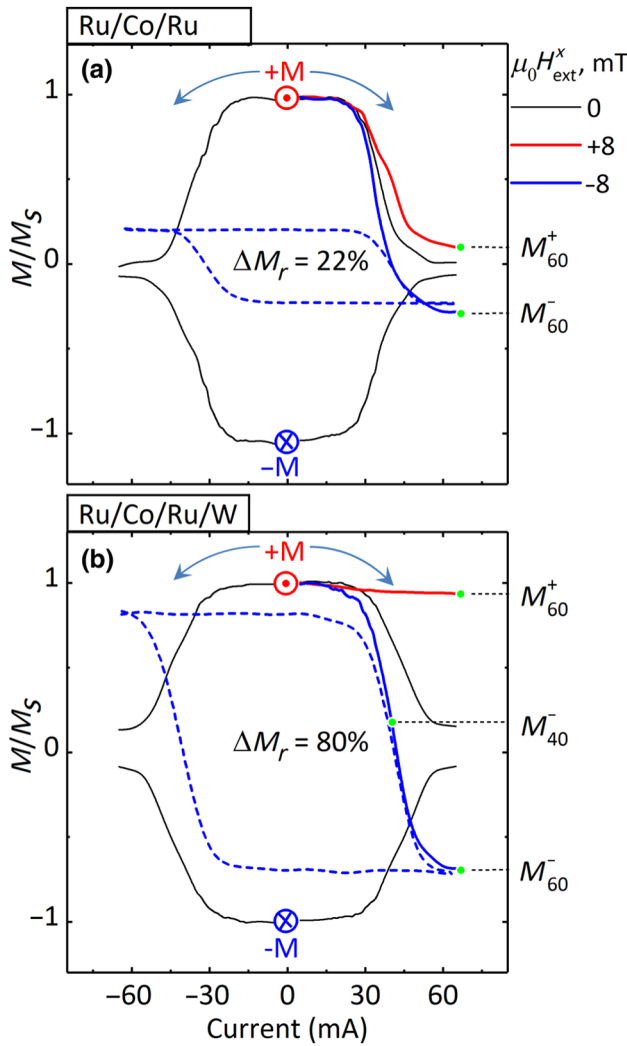
FIG. 3. A set of demagnetization curves obtained by passing the current of increasing amplitude after preliminary magnetization to the saturation state with a different value of the in-plane field $\mu_0 H_{ext}^x$ for Ru/Co/Ru (a) and Ru/Co/Ru/W (b). Current-induced magnetic hysteresis loops allow determining the switching amplitude.

$j_{max} \approx 2 \times 10^{11}$ A/m^2. The measured value of AHE is proportional to the change in the sample magnetization (M). The maximum value of AHE corresponds to the saturation state with $\pm M_s$ and it is minimal when $M \to 0$, i.e., in a demagnetized state. For a better presentation of the data, we use reduced M/M_s values proportional to AHE. The results of measuring AHE in $\mu_0 H_{ext}^x = 0$ are indicated by the black line in Fig. 3. It can be seen that with increasing current amplitude, the sample's magnetization $\pm M_s$ decreases sharply at the current of ± 30 mA and reaches saturation when $I = \pm 55$ mA and $M \to 0$.

The measurements are repeated for four combinations of the orientation of the initial magnetization $\pm M_s$ and the current direction $\pm I$. In all cases, the magnitude of the

residual magnetization M_r is the same in magnitude, which indicates the homogeneity of the system and the absence of effective magnetic fields $\mu_0 H_{SOT}^z$.

The results of visualization of the magnetization reversal process by the current for both structures are shown in Fig. 4. Several differences should be noted between the conclusions on the magnetization reversal process defined from the magnetization reversal curves and the corresponding Kerr microscopy images. As it can be seen from the Kerr images for both samples with the passing current $I = 60$ mA in the Hall bar, the area of the domains magnetized up and down is approximately the same, which is associated with the action of the nonuniform Oersted field. At the same time, the found values of M_r on the demagnetization curves (Fig. 3) do not reach zero due to the nonuniform switching of the magnetization in the transverse part of the Hall bar. In Fig. 4 for the case $I = +60$ mA, it can be seen that there is a bright contrast in the lower transverse part of the Hall bar and only a dark contrast in the upper one. This asymmetry in the transverse part of the Hall bar leads to a small magnitude of M_r not equal to 0.

Comparing the magnetization reversal curves for the samples with and without W, it can be noted that, despite the different values of the coercive force, the change in the magnetization from the saturation state occurs approximately at the same current values. Presumably, this is due to the fact that the magnetization switching starts from the uniform edges of the Hall bar as will be illustrated later in Fig. 8. In the area of the Hall cross, due to current spreading, the Oersted field is much smaller. Exit of the AHE curves from the saturation state at the same current is due to the fact that the area of the Hall cross, where the level of the AHE signal depends on the magnetization, begins to switch earlier in the Ru/Co/Ru structure, because of the presence of the interfacial Dzyaloshinskii-Moriya interaction (DMI) [11], as will be shown below.

2. Current-induced magnetization reversal in an external field $\mu_0 H_{ext}^x = \pm 8$ mT

As in the previous experiment, the sample is magnetized to the saturation state with an external field $\mu_0 H_{ext}^z$, after which it is turned off. However, now the current pulses are applied in the presence of an in-plane magnetic field oriented parallel to the current direction. In this case, the M_r value after passing the current depends on its direction.

In the case of the Ru/Co/Ru structure, if the directions of the current and the field coincide, the region of the microstrip, in which the magnetization is switched, decreases to M_{60}^+ as compared with the case $\mu_0 H_{ext}^x = 0$ [Fig. 3(a)]. If the directions of the current and the field are opposite, the switching region is increased to M_{60}^-. Such a change is associated with the appearance of a nonzero effective field $\mu_0 H_{SOT}^z$, due to the SOT effect. Unlike the
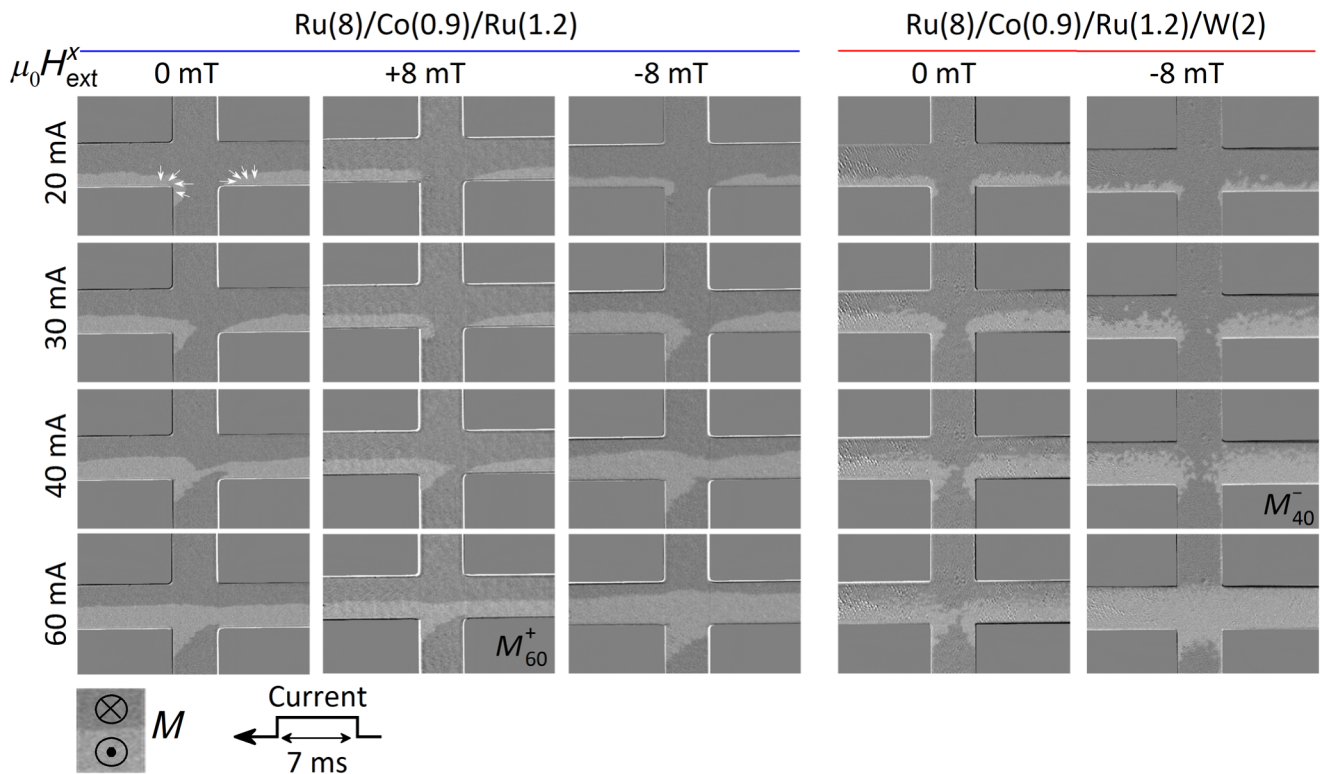
FIG. 4. Changes in the domain structure during the current-induced magnetization reversal of Ru/Co/Ru and Ru/Co/Ru/W samples for different values of the field $\mu_0 H^x_{ext}$.

Oersted field, whose z component on opposite sides of the microstrip has the opposite orientation, the SOT effect field has the same orientation over the entire area of the microstrip, due to the direction of magnetization tilt caused by action of the field $\mu_0 H^x_{ext}$ and by the direction of the spin current [37].

As seen in the Kerr microscopy images in Fig. 4 for the Ru/Co/Ru/W structure, the current passing in the presence of the field $\mu_0 H^x_{ext} = -8$ mT leads to a complete switching of the magnetization [blue curve in Fig. 3(b)]. In the field $\mu_0 H^x_{ext} = +8$ mT, no change in the magnetization is observed [red line in Fig. 3(b)]. The illustration is not given for this case, since there is no change in the magnetic structure.

3. Current-induced magnetization reversal in the presence of a constant field $\mu_0 H^x_{ext}$, but without preliminary magnetization by an external magnetic field to the saturation state

By applying current pulses from -60 to $+60$ mA, we obtain current-induced hysteresis loops (marked by dashed lines in Fig. 3), in which the magnetization varies from M^+_{60} to M^-_{60}. At the same time, the change in magnetization ΔM_r is 22% for the Ru/Co/Ru sample during the complete magnetization reversal of the structure from the saturation state and 80% for the Ru/Co/Ru/W sample.. However, to

define that the current-induced magnetization reversal is incomplete, one has to visually observe the domain structure. In many previous studies based on the measurement of AHE loops, this fact was not verified.

A change in the orientation of the field $\mu_0 H^x_{ext}$ leads to a symmetric reversal of the loop, which is characteristic of the magnetization reversal through the SHE mechanism [38]. For all the samples considered in the work, it is found that applying an external field $\mu_0 H^y_{ext}$ orthogonal to the current direction does not lead to the appearance of a current-induced field $\mu_0 H^z_{SOT}$. Based on this fact, it can be concluded that in the considered system only the longitudinal dampinglike field (DL) [37] is responsible for switching. Therefore, when describing the effective fields of the SOT effect, instead of $\mu_0 H_{SOT}$, we use the notation $\mu_0 H_L$.

Considering the details of the magnetization reversal process of the Ru/Co/Ru sample, it can be noted that the domain growth takes place asymmetrically and the domain wall itself has a smooth profile as compared with the sample containing the W layer. We assume that these features are associated with the presence of DMI in the sample. An asymmetric propagation of the domain wall in the Hall cross area was observed earlier [21,39,40]. The presence of DMI allows stabilizing of the homochiral Neel domain walls. As a result, domain walls located on different sides of the Hall cross have vertical segments with the opposite

orientation of the magnetization along the x axis (upper left image in Fig. 4). In this case, the effective field of the SOT effect depends on the mutual orientation of the polarization of the spin current σ (y axis) and the local distribution of the magnetization m: $\mu_0 H_L \sim \sigma \times m$. This result leads to the fact that the resulting field of the SOT effect has a different direction relative to the domain walls on opposite sides of the Hall cross. The action of such a field leads to the expansion of the domain along the x axis from one side. In our previous study, the value of DMI $D = -0.2$ mJ/m^2 is measured in the Ru/Co/Ru trilayer [11]. This value is due to the partial oxidation of the top Ru layer, leading to uncompensated DMI from the bottom and top interfaces. In contrast, the Ru/Co/Ru/W system has about zero DMI, because the W capping prevents the oxidation of the top Ru, resulting in complete DMI compensation from the bottom and top interfaces.

The above study leads to the following conclusions. (i) In the considered structures, the magnetization switching under the action of the current always starts from the edge and, as the amplitude of the current increases, the domain wall moves parallel to the edge of the Hall bar. (ii) Measurement of AHE does not allow us to unambiguously judge the behavior of the magnetization and the degree of saturation of the sample. To illustrate this, one can compare two cases M_{60}^+ and M_{40}^- (Fig. 4) with the corresponding levels of the AHE signals (Fig. 3). (iii) The sign of the effective field of the SOT effect is the same in both samples. (iv) Addition of the W layer in the considered structure enables a complete magnetization switching under the action of the current.

B. Quantitative evaluation of current-induced magnetization reversal

For a quantitative description of the studied structures, an estimation of the effective magnetic fields generated by passing a current is made. The study shows that determining this value for low-coercive samples with a small value of the PMA energy is a nontrivial task. In the following, we consider three approaches to determine the current-induced effective field.

1. Second harmonic generation measurement method

The harmonic Hall voltage measurement [41] is the generally accepted method for determining the SOT effect efficiency. While changing the magnitude of the external magnetic field $\mu_0 H_{\text{ext}}^x$, an alternating current is passed through a Hall bar and the transverse potential difference of AHE is recorded at the excitation frequency V_ω and at the double frequency $V_{2\omega}$. The analytical model [17] describing this process allows us to determine the magnitude of the current-induced effective field $\mu_0 H_L$, in the simplest case, by the formula

$$\mu_0 H_L = -2 \left(\frac{dV_{2\omega}}{\mu_0 dH_{\text{ext}}^x} \right) \Big/ \left(\frac{d^2 V_\omega}{\mu_0 dH_{\text{ext}}^{2x}} \right). \quad (1)$$

Using this approach, experimental dependencies of the AHE response on the first and second harmonics are obtained for the samples considered in this paper (Fig. 5). During measurements, an alternating current with an amplitude of 10 mA and a frequency of 17 Hz is applied to the samples and the external magnetic field is changed along the current direction. The key parameter of these measurements is the slope of the linear segment of the second harmonic near zero field, since it corresponds to the magnitude of the magnetization deflection under the current action. It is seen that the addition of the W layer leads to a sharp increase in the slope, which indicates a significant increase in the effectiveness of the current action on the magnetization (Fig. 5). For the numerical estimate of the effective field, in addition to the slope, the curvature of the first harmonic is determined. It is found that a change in the external field in the range of ± 100 mT leads to a partial demagnetization of the sample, which makes the resulting dependence incorrect. To study the response from the saturated state, the sample is preliminarily magnetized by an external perpendicular field, after which it is turned off, and the measurement is performed in the in-plane field range $\mu_0 H_{\text{ext}}^x = \pm 20$ mT. As it can be seen in Fig. 5, such an approach allows one to define very different values of the level and curvature of the first harmonic
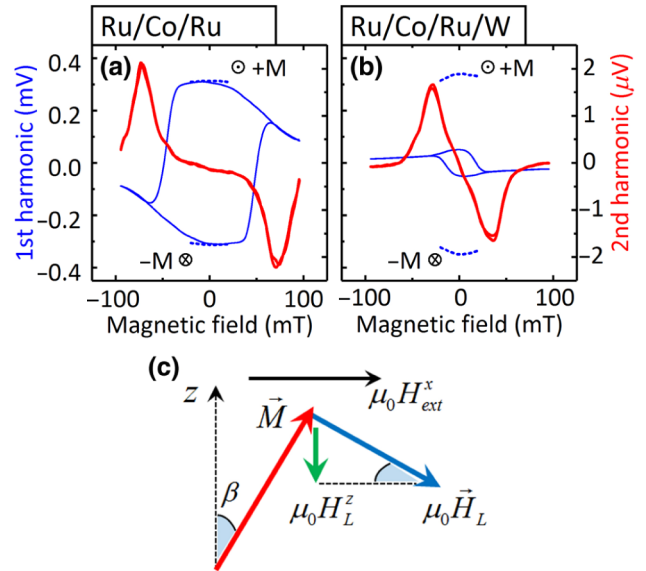

FIG. 5. Dependence of the AHE amplitude on the magnitude of the in-plane field applied along the current direction at the first and second harmonics for structures without W (a) and with W (b). The signal at the first harmonic is also measured in a field range of ± 20 mT after the preliminary magnetization (dashed lines). (c) Scheme of mutual orientation of the magnetization, the effective field of SOT effect, and its projection on the z axis.

dependence (blue dashed lines). It can be assumed that the demagnetization of the samples is due to the small value of the effective field of PMA and a relatively large alternating current, while the combination of the external field and the induced field of the SOT effect is sufficient for demagnetization. For the case of the structure containing the W layer, where the SOT effect field is obviously larger, the demagnetization turns out to be stronger.

Using formula (1), we find the values of the effective field $\mu_0 H_L$ equal to 3 and 6 mT at the current of 60 mA for structures without and with W, respectively. The resulting field is oriented perpendicular to the magnetization, as shown in Fig. 5(c). Considering the magnitude of the anisotropy field (Table I) and the conditions of the previously described experiment (Fig. 3), we can estimate the angle $\beta = 3.3°$ and $7.6°$ for the first and second structures, respectively. The projection of the $\mu_0 H_L$ field on the z axis gives the corresponding values of $\mu_0 H_L^z$ equal to 0.13 and 0.8 mT. Comparing these values with magnetic hysteresis loops [Fig. 1(b)], it can be seen that there are not enough such fields for complete magnetization reversal as is observed in the sample containing the W layer, especially when considering the oppositely directed Oersted field. Thus, the second harmonic generation method does not allow us to determine real values of the effective fields induced by a passing current.

2. Current-induced magnetization curve method

A qualitatively different approach for determining the effective field induced by the SOT effect is based on recording the magnetization curves [20]. The Ru/Co/Ru/W sample is demagnetized by an in-plane alternating field and then saturated in one case by means of an external perpendicular field [Fig. 6(a)] and in another by passing a current in the presence of a small planar field [Fig. 6(b)]. Analyzing two magnetization curves, we can assume that the work on magnetization (Zeeman energy) in both cases should be the same:

$$E_z^H = M_s \int_0^1 \mu_0 H_{\text{ext}}^z dM_n, \tag{2}$$

$$E_z^I = M_s A \int_0^1 I dM_n, \tag{3}$$

where M_n is the normalized value of magnetization. Since the field induced by the current linearly depends on the current magnitude I, we can represent the effective field as $\mu_0 H_L^z = AI$. Equating expressions (2) and (3), we can find the proportionality coefficient between the field and the current, which is equal to the ratio of the areas S_B and S_I corresponding to the red and blue areas in Fig. 6. The presented measurements are carried out only for the Ru/Co/Ru/W structure, since for the structure without W
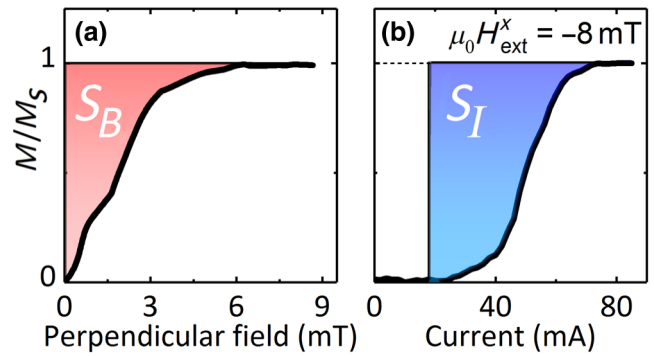

FIG. 6. Magnetization curves of the Ru/Co/Ru/W structure measured under the action of the field (a) and current (b).

it is impossible to obtain a saturation state by means of current. As seen in Fig. 6(b), at the initial stage, the application of current does not lead to the exit from the saturation state. It can be assumed that this is due to the action of the nonuniform Oersted field, under the action of which the domains with different magnetization orientations are redistributed in the microstrip, while the resulting value of the magnetization remains zero. This process cannot be illustrated using Kerr microscopy. However, it can be noted that, at the initial stage, the work on magnetization is not performed, so we did not consider the area above the zero magnetization value. This approach allows us to define the value $\mu_0 H_L^z = 4.4$ mT, which, taking into account the mutual orientation of the fields, as in Fig. 5(c), gives the value of the effective field $\mu_0 H_L = 33.8$ mT.

The action of such a field could lead to a complete magnetization switching; however, the considered method does not allow determining the value of the effective field in the sample without the W layer. For this purpose, we propose an alternative approach.

3. Method of analyzing the domain-wall position

Analyzing the demagnetization process of Hall bars of both compositions under the current action in the absence of an external field (Fig. 4), we can draw two conclusions. (i) The magnitude of the Oersted field generated by the current of the amplitude considered is greater than the magnitude of the coercive force of the both samples. This conclusion leads to the fact that the magnetization reversal occurs by moving the domain wall parallel to the long side of the Hall bar (perpendicular to the current). (ii) This movement under the action of the nonuniform Oersted field will continue to the point where the field value becomes zero, that is, to the middle of the Hall bar.

In the presence of an external field $\mu_0 H_{\text{ext}}^x$, the character of the magnetization reversal does not change: an increase in the current amplitude leads to parallel movement of the domain wall, but now, depending on the direction of the external field, the final position of the domain wall will

be on opposite sides relative to the middle of the Hall bar. Such a change is associated with the appearance of an additional magnetic field $\pm\mu_0 H_L$, induced by the SOT effect, which is superimposed on the nonuniform Oersted field. It can be assumed that the movement of the domain wall will continue as before to the region with zero value of the resulting magnetic field; then the condition for the position of the domain wall can be written in the form

$$\mu_0 H_{\text{Oe}} \pm \mu_0 H_L = 0. \qquad (4)$$

The arguments presented correspond well to the behavior of the domain structure of the Ru/Co/Ru sample (Fig. 4).
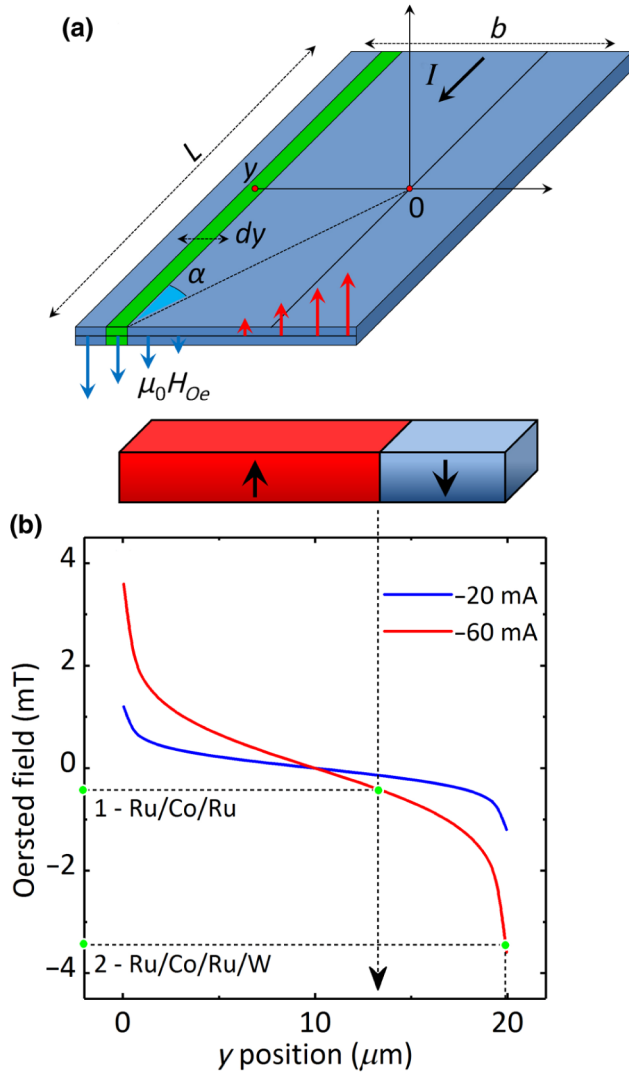

FIG. 7. (a) Calculation scheme for the Oersted field on a homogeneous section of the Hall bar. (b) The calculated distribution of the Oersted field in the cross section of the microstrip, perpendicular to the current direction. The vertical dashed lines mark the position of the domain wall for two structures after passing the maximum current into the presence of an external field $\mu_0 H_{\text{ext}}^x = 8$ mT.

The profile of the domain wall in the sample with W ceases to be smooth, which casts doubt on the applicability of the model described above, but the final conclusions can be applied to it.

Using condition (4), one can determine the SOT effect effective field, if one knows the position of the domain wall and the spatial distribution of the Oersted field. It can be noted that the magnitude and distribution of the Oersted field depend only on the geometry of the microstrip and the current strength. For further consideration, an analytical expression for the distribution of the Oersted field is obtained. Without considering the area of the Hall bar's crossline, we can assume that the current density is uniform over the cross section of the microstrip. Let us consider a microstrip of length L and width b [Fig. 7(a)]. We divide the microstrip into infinitely thin conductors with width dy parallel to the current direction. Based on the Biot-Savart-Laplace law [Eq. (5), where $\vec{r}$, in general, is a radius vector between a current element dl and a point, where the field is calculated], one can obtain an expression for the magnetic field $\mu_0 H_{\text{Oe}}$ oriented perpendicular to the microstrip plane [Eq. (6)]:

$$\mu_0 dH_{\text{Oe}} = \frac{\mu_0}{4\pi} \frac{I(\vec{dl} \times \vec{r})}{r^3}, \qquad (5)$$

$$\mu_0 dH_{\text{Oe}} = \frac{\mu_0}{2\pi} \frac{dI}{y} \cos\alpha. \qquad (6)$$

Equation (6) allows calculating the field value across the center of a conductor of length L with the current dI in a point at a distance y. One can express the magnitude of the current passing through the elementary conductor through
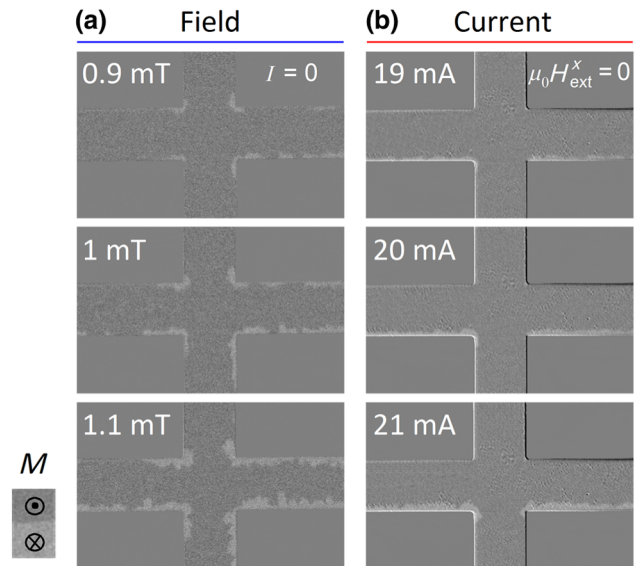

FIG. 8. Kerr microscopy illustration of the initial stage of the Ru/Co/Ru/W Hall bar demagnetization under the action of the perpendicular magnetic field (a) and current (b).

its width: $dI = (I/b)dy$. Each conductor contributes to the resulting magnetic field at point y:

$$
\mu_0 dH_{\text{Oe}} = \frac{\mu_0 I}{2\pi b} \frac{1}{y} \cos\alpha\, dy = \frac{\mu_0 I}{2\pi b} \frac{1}{y} \frac{dy}{\sqrt{1 + \tan^2\alpha}}
$$

$$
= \frac{\mu_0 I}{2\pi b} \frac{1}{y} \frac{dy}{\sqrt{1 + [y^2/(L/2)^2]}}, \qquad (7)
$$

where, in accordance with the scheme of Fig. 7(a), we move from $\cos\alpha$ to distance parameters. Further, it is considered that the parts of the microstrip located on opposite sides of the point y contribute with the opposite sign to the resulting magnetic field. Considering this contribution when integrating, one can get

$$
\mu_0 H_{\text{Oe}} = \frac{\mu_0 I L}{4\pi b} \left[\int_y^0 \frac{1}{y\sqrt{(L/2)^2 + x^2}} dy \right.
$$

$$
\left. - \int_{b-y}^0 \frac{1}{y\sqrt{(L/2)^2 + y^2}} dy \right]
$$

$$
= \frac{\mu_0 I}{2\pi b} \ln\left[\frac{(L/2) + \sqrt{(L/2)^2 + (b-y)^2}}{(L/2) + \sqrt{(L/2)^2 + y^2}} \frac{y}{b-y} \right].
$$

$$(8)$$

This dependence describes the distribution of the z component of the Oersted field in a cross section of the microstrip perpendicular to the current direction. The calculation for different cases of length L shows that the condition $L \gg b$ is met for the experimentally considered Hall bars. With this in mind, the expression (8) is reduced to the form

$$
\mu_0 H_{\text{Oe}} = \frac{\mu_0 I}{2\pi b} \ln\left(\frac{y}{b-y}\right). \qquad (9)
$$

An analysis of expression (9) shows that when approaching the microstrip edges, the field value starts to increase asymptotically, so the maximum field depends on the area of homogeneity (step) along the y axis. A calculation of the Oersted field distribution for two current values at a step of 50 nm is given in Fig. 7(b). The obtained distribution qualitatively and quantitatively coincides with the distribution found by the simulation method as in Ref. [22]. To verify the compliance of the calculation results with the experiment, the demagnetization of the Hall bar at the initial stage is considered. The visualization of the change in the magnetic structure of the Ru/Co/Ru/W sample when exiting from the saturation state under the action of an external perpendicular field is shown in Fig. 8(a). The structure with the W layer is considered due to the fact that the demagnetization process in it begins from the edges, whereas in the

Ru/Co/Ru sample it begins from the middle. This case is compared to the case of demagnetization under the current action in the absence of an external field, that is, under the Oersted field action only [Fig. 8(b)]. Roughly, the effects of 1 mT and 20 mA are comparable. However, the current generates the Oersted field, which is nonuniform. On one hand, its orientation is codirected with the Hall bar magnetization and does not cause changes. On the other hand, at the lower edge of the Hall bar, the generated field orientation is opposite to the magnetization direction, which leads to local magnetization reversal [Fig. 8(b)]. The distribution of the Oersted field for 20 mA is given in Fig. 7(b) and, at the edge of the microstrip, it corresponds to a field of 1.2 mT. With such a comparison, an exact value cannot be found due to a number of factors: the nonuniformity of the Oersted field, the uncertainty of its magnitude at the edges, heating from the current, etc. However, for a rough estimate, we try to apply the analytically defined distribution.

Describing the position of the domain wall by condition (4), we can conclude that it will stop at the place of the Hall bar cross section, where the z component of the SOT field is modulo the Oersted field. Knowing the value of the Oersted field at each point of the Hall bar and determining the position of the domain wall using Kerr microscopy (Fig. 4), one can determine the field $\pm\mu_0 H_L$. For the sample without W, passing a current of 60 mA in the presence of a field of $+8$ and -8 mT gives the domain wall offset from the lower edge by 8.2 and 12.3 μm, respectively. The value of the Oersted field and, hence, the resultant field of the SOT effect in these places is -0.25 and $+0.31$ mT. In one case, the SOT effect field helps to exit from the saturation magnetization state; in the other case, it prevents an exit. The difference in values is due to the ambiguity of determining the position of the domain wall due to the nonlinearity of the boundary. The average value of the z component of the induced field is 0.28 mT; considering the magnetization tilting angle, the magnitude of the effective field is 4.9 mT.

As mentioned earlier, the external in-plane field of -8 mT is minimal for achieving a complete magnetization switching of the structure with W. With this field $\mu_0 H_{\text{ext}}^x$, the SOT effect field is everywhere larger than the Oersted field, i.e., $\mu_0 H_L^z \geq 3.6$ mT. The corresponding value of the SOT effect effective field in the structure with W is 27.7 mT.

C. Comparison of results

The values of the effective fields found by different methods are given in Table II. It can be seen that for the Ru/Co/Ru structure, the harmonic method and the method based on the distribution of the Oersted field are in good agreement. The results for the structure with the W layer are more scattered. For the final evaluation of the

TABLE II.   The values of the effective fields $\mu_0 H_L$ (and their projections on the z axis, $\mu_0 H_L^z$) in mT, determined by three methods for samples of two compositions, and the SOT efficiency.

| Sample | Methods of definition of $\mu_0 H_L$ ($\mu_0 H_L^z$) (mT) | | | γ_L (10^{-11} mT/Am^{-2}) | ξ_L |
	Second harmonic	Magnetization curve	Domain-wall position		
Ru/Co/Ru	3 (0.13)	...	4.9 (0.28)	1.6	0.03
Ru/Co/Ru/W	6 (0.8)	33.8 (4.4)	27.7 (3.6)	9.2	0.15

SOT effect in our structures, the values determined by the third method (domain-wall position) are considered, since it is the most direct approach for the evaluation of the current-induced field.

The discrepancy between the effective fields measured by different methods confirms that there is no universal measurement method and it is necessary to verify the correctness of the used method for each particular system under study. In particular, our results demonstrate that the harmonic measurement method is not suitable for the study of low-coercive samples.

For the considered systems, the coefficient showing the ratio of the magnitude of the induced field to the current γ_L and the SOT efficiency ξ_L (effective angle of SHE) are calculated. The value of the SOT efficiency can be used for comparing the SOT effects in different structures [42]:

$$\xi_L = \frac{2e}{\hbar} \mu_0 M_s t_{Co}^{eff} \left| \frac{H_L}{j} \right| , \qquad (10)$$

where e and $\hbar$ are the elementary charge and the Dirac constant, respectively. This value reflects the ratio of the spin current density adsorbed by a ferromagnetic layer to the charge current injected into a heavy-metal layer. The values of current density j and effective field $\mu_0 H_L$ are substituted by values experimentally defined for $I = 60$ mA. The effective thickness of the ferromagnetic layer is determined as the thickness of the Co layer equal to 0.5 nm, taking into account the magnetic dead layer of 0.2 nm at each interface with Ru [43].

Assuming that the top Ru layer thickness is 1.2 nm and its contribution to the SOT effect is negligible, the efficiency of the Ru buffer layer is $\xi_L^{Ru} = 0.03$. Comparison of the defined value with previous works is difficult because very few papers are devoted to the study of the SOT effect in structures with Ru. We can point out the study of the epitaxial Ru/CoFeAl/MgO structure [10]. It is shown that with increasing thickness of the Ru buffer layer in the range up to 8 nm, the SOT effect effective fields increase, reaching maximum values of $\mu_0 H_L/j = 0, 2 \times 10^{-11}$ mT/Am^{-2} and $\mu_0 H_T/j = 0, 5 \times 10^{-11}$ mT/Am^{-2} with the maximum SOT efficiency $\xi_j = 0.0056$. The transverse (fieldlike, H_T) field turns out to be larger than the longitudinal (antidampinglike, H_L), whereas in our work it is not detected at all, while the

value of the longitudinal field in the Ru/Co/Ru structure is almost an order of magnitude larger.

Considering the measured value of ξ_L^{Ru}, the SOT efficiency of the W layer in the Ru/Co/Ru/W structure is $\xi_L^W = 0.12$. The presence of an intermediate Ru/Co interface leads to additional screening due to the high spin-memory-loss parameter $\delta_{Co/Ru} = 0.34$ [44,45], so the value of ξ_L^W is slightly less than the previously defined data for the mixed $\alpha + \beta$ crystalline phase of W: $\xi_L^W = 0.18$ [26].

IV. CONCLUSIONS

An experimental study of the current-induced magnetization reversal of the Ru/Co/Ru and Ru/Co/Ru/W structures has been performed. In both structures, only a longitudinal field (antidumpinglike) is generated; the ratios of the effective field to the current and the SOT efficiency are 1.6×10^{-11} mT/Am^{-2} and 0.03 for the sample without W and 9.2×10^{-11} mT/Am^{-2} and 0.15 for the sample with W. It is shown that the determination of the magnitude of the SOT effect effective fields in samples with small values of the coercive force and the anisotropy field is a nontrivial problem. Observation of the domain structure during the magnetization reversal process allows explaining the features on the AHE loops. It is hard to accurately judge the magnetization behavior inside a Hall bar and the degree of magnetization saturation of the sample from the AHE loops. A direct method for estimating the magnitude of the SOT effect field is proposed based on the analysis of the domain-wall position in the case of its displacement parallel to the current combined with the spatial distribution of the Oersted field. It is shown that, for the implementation of the SOT effect, one can use an additional $5d$ metal layer with a strong SHE, while the rest of the structure, based on $4d$ metals, determines the magnetic parameters of the ferromagnetic layer. The advanced method for estimation of the SOT effect efficiency in low-coercivity ferromagnetic multilayers can be adopted to a wide spectrum of materials, including Pt-based systems.

Moreover, we demonstrate that the modified Ru-based systems with PMA are very promising candidates to be used in spin orbitronics as an alternative to mainstream Pt-based systems. It is noteworthy that Ru-based systems have a one-order-smaller Gilbert damping parameter compared to Pt-based systems [46]. This fact makes the

Ru-based systems attractive also for rf applications and skyrmion-based racetrack memory.

ACKNOWLEDGMENTS

[1] I. M. Miron, K. Garello, and P. Gambardella, Perpendicular switching of a single ferromagnetic layer induced by in-plane current injection, Nature **476,** 189 (2011).

[2] K. Cai, M. Yang, and K. Wang, Electric field control of deterministic current-induced magnetization switching in a hybrid ferromagnetic/ferroelectric structure, Nat. Mater. **16,** 712 (2017).

[3] Y. Sheng, K. W. Edmonds, and K. Wang, Adjustable current-induced magnetization switching utilizing interlayer exchange coupling, Adv. Electron. Mater. **4,** 1800224 (2018).

[4] Y. Cao, A. Rushforth, and K. Wang, Tuning a binary ferromagnet into a multistate synapse with spin–orbit-torque-induced plasticity, Adv. Funct. Mater. 1808104 (2019).

[5] W. J. Kong, C. H. Wan, and X. F. Han, Spin–orbit torque switching in a T-type magnetic configuration with current orthogonal to easy axes, Nat. Commun. **10,** 233 (2019).

[6] C. O. Avci, K. Garello, and P. Gambardella, Fieldlike and antidamping spin-orbit torques in as-grown and annealed Ta/CoFeB/MgO layers, Phys. Rev. B **89,** 214419 (2014).

[7] T. Wang, J. Q. Xiao, and X. Fan, Spin–orbit torques in metallic magnetic multilayers: Challenges and new opportunities, SPIN **7,** 1740013 (2017).

[8] X. Qiu, Z. Shi, and H. Yang, Characterization and manipulation of spin orbit torque in magnetic heterostructures, Adv. Mater. **30,** 1705699 (2018).

[9] P. Gambardella and I. M. Miron, Current-induced spin–orbit torques, Philos. Trans. R. Soc., A **369,** 3175 (2011).

[10] Z. Wen, J. Kim, and S. Mitani, Spin-orbit torque in Cr/CoFeAl/MgO and Ru/CoFeAl/MgO epitaxial magnetic heterostructures, AIP Adv. **6,** 056307 (2016).

[11] A. Samardak, A. Kolesnikov, and A. Ognev, Enhanced interfacial Dzyaloshinskii-Moriya interaction and isolated skyrmions in the inversion-symmetry-broken Ru/Co/W/Ru films, Appl. Phys. Lett. **112,** 192406 (2018).

[12] Y. Jijun, L. Dong, and X. Li, Current induced domain wall motion and tilting in Pt/Co/Ta structures with perpendicular magnetic anisotropy in the presence of the Dyzaloshinskii–Moriya interaction, J. Phys. D: Appl. Phys. **51,** 155001 (2018).

[13] J. Yu, X. Qiu, and H. Yang, Large spin-orbit torques in Pt/Co-Ni/W heterostructures, Appl. Phys. Lett. **109,** 042403 (2016).

[14] J. Kim, J. Sinha, and H. Ohno, Layer thickness dependence of the current-induced effective field vector in Ta|CoFeB|MgO, Nat. Mater. **12,** 240 (2012).

[15] A. Ghosh, K. Garello, and P. Gambardella, Interface-Enhanced Spin-Orbit Torques and Current-Induced Magnetization Switching of Pd/Co/AlOx Layers, Phys. Rev. Appl. **7,** 014004 (2017).

[16] S. K. Li, X. T. Zhao, and Z. D. Zhang, Enhanced spin-orbit torques and perpendicular magnetic anisotropy in CoFeB/MgO structures with Ta/W bilayer, AIP Adv. **8,** 065007 (2018).

[17] M. Hayashi, J. Kim, and H. Ohno, Quantitative characterization of the spin-orbit torque using harmonic Hall voltage measurements, Phys. Rev. B **89,** 144425 (2014).

[18] X. Qiu, P. Deorani, and H. Yang, Angular and temperature dependence of current induced spin-orbit effective fields in Ta/CoFeB/MgO nanowires, Sci. Rep. **4,** 4491 (2014).

[19] C.-F. Pai, M. Mann, and G. S. D. Beach, Determination of spin torque efficiencies in heterostructures with perpendicular magnetic anisotropy, Phys. Rev. B **93,** 144409 (2016).

[20] T. Koyama, Y. Guan, and D. Chiba, Investigation of spin-orbit torque using current-induced magnetization curve, Sci. Rep. **7,** 790 (2017).

[21] J. Cao, Y. Chen, and W. S. Lew, Spin orbit torques induced magnetization reversal through asymmetric domain wall propagation in Ta/CoFeB/MgO structures, Sci. Rep. **8,** 1355 (2018).

[22] C. J. Durrant, R. J. Hicken, and G. Xiao, Scanning Kerr microscopy study of current-induced switching in Ta/CoFeB/MgO films with perpendicular magnetic anisotropy, Phys. Rev. B **93,** 014414 (2016).

[23] A. G. Kolesnikov, M. E. Stebliy, and L. A. Chebotkevich, Enhancement of perpendicular magnetic anisotropy and coercivity in ultrathin Ru/Co/Ru films through the buffer layer engineering, J. Phys. D: Appl. Phys. **49,** 425302 (2016).

[24] M. Yang, K. Cai, and K. Wang, Spin-orbit torque in Pt/CoNiCo/Pt symmetric devices, Sci. Rep. **6,** 20778 (2016).

[25] H. An, H. Nakayama, and K. Ando, Spin-orbit torques in asymmetric Pt/Co/Pt structures, Phys. Rev. B **94,** 214417 (2016).

[26] C.-F. Pai, L. Liu, and R. A. Buhrman, Spin transfer torque devices utilizing the giant spin Hall effect of tungsten, Appl. Phys. Lett. **101,** 122404 (2012).

[27] Y. Satoshi, A. Yasuo, and M. Shigemi, Temperature dependences of spin-diffusion lengths of Cu and Ru layers, Jpn. J. Appl. Phys. **45,** 3892 (2006).

[28] W. Zhang, V. Vlaminck, and A. Hoffmann, Determination of the Pt spin diffusion length by spin-pumping and spin Hall effect, Appl. Phys. Lett. **103**, 242414 (2013).

[29] G. W. Kim, A. S. Samardak, and Y. K. Kim, Role of the Heavy Metal's Crystal Phase in Oscillations of Perpendicular Magnetic Anisotropy and the Interfacial Dzyaloshinskii-Moriya Interaction in W/CoFeB/MgO Films, Phys. Rev. Appl. **9**, 064005 (2018).

[30] J. Liu, T. Ohkubo, and M. Hayashi, Correlation between the spin Hall angle and the structural phases of early 5d transition metals, Appl. Phys. Lett. **107**, 232408 (2015).

[31] Q. Hao and G. Xiao, Giant Spin Hall Effect and Switching Induced by Spin-Transfer Torque in a W/Co40Fe40B20/ MgO Structure with Perpendicular Magnetic Anisotropy, Phys. Rev. Appl. **3**, 034009 (2015).

[32] Q. Hao, W. Chen, and G. Xiao, Beta (β) tungsten thin films: Structure, electron transport, and giant spin Hall effect, Appl. Phys. Lett. **106**, 182403 (2015).

[33] S. M. Rossnagel, I. C. Noyan, and C. Cabral, Phase transformation of thin sputter-deposited tungsten films at room temperature, J. Vac. Sci. Technol., B: Nanotechnol. Microelectron.: Mater., Process., Meas., Phenom. **20**, 2047 (2002).

[34] P. Sheng, Y. Sakuraba, and M. Hayashi, The spin Nernst effect in tungsten, Sci. Adv. **3**, e1701503 (2017).

[35] C. A. F. Vaz and J. A. C. Bland, Dependence of the coercive field on the Cu overlayer thickness in thin Co/Cu(001) and Ni/Cu(001) fcc epitaxial films, J. Appl. Phys. **89**, 7374 (2001).

[36] I. Tabakovic, V. Inturi, and S. Riemer, Composition, structure, stress, and coercivity of electrodeposited soft magnetic CoNiFe films: Thickness and substrate dependence, J. Electrochem. Soc. **149**, C18 (2002).

[37] K. Garello, I. M. Miron, and P. Gambardella, Symmetry and magnitude of spin–orbit torques in ferromagnetic heterostructures, Nat. Nanotechnol. **8**, 587 (2013).

[38] L. Liu, O. J. Lee, and R. A. Buhrman, Current-Induced Switching of Perpendicularly Magnetized Magnetic Layers Using Spin Torque from the Spin Hall Effect, Phys. Rev. Lett. **109**, 096602 (2012).

[39] J. Yu, X. Qiu, and H. Yang, Spin orbit torques and Dzyaloshinskii-Moriya interaction in dual-interfaced Co-Ni multilayers, Sci. Rep. **6**, 32629 (2016).

[40] J. C. Rojas-Sánchez, P. Laczkowski, and J. M. George, Perpendicular magnetization reversal in Pt/[Co/Ni]$_3$/Al multilayers via the spin Hall effect of Pt, Appl. Phys. Lett. **108**, 082406 (2016).

[41] U. H. Pi, K. Won Kim, and S. Seo, Tilting of the spin orientation induced by Rashba effect in ferromagnetic metal layer, Appl. Phys. Lett. **97**, 162507 (2010).

[42] C.-F. Pai, Y. Ou, and R. A. Buhrman, Dependence of the efficiency of spin Hall torque on the transparency of Pt/ferromagnetic layer interfaces, Phys. Rev. B **92**, 064426 (2015).

[43] A. G. Kolesnikov, A. V. Ognev, and A. S. Samardak, Nanoscale control of perpendicular magnetic anisotropy, coercive force and domain structure in ultrathin Ru/Co/ W/Ru films, J. Magn. Magn. Mater. **454**, 78 (2018).

[44] M. A. Khasawneh, C. Klose, and N. O. Birge, Spin-memory loss at Co/Ru interfaces, Phys. Rev. B **84**, C18 (2011).

[45] Y. Wu, K. Meng, and Y. Jiang, Enhanced spin-orbit torque in Pt/Co/Pt multilayers with inserting Ru layers, J. Magn. Magn. Mater. **472**, 14 (2019).

[46] P. Neilinger, T. Ščepka, and V. Cambel, Ferromagnetic resonance study of sputtered Pt/Co/Pt multilayers, Appl. Surf. Sci. **461**, C18 (2018).